AIAA SCITECH 2024 Forum, 8-12 January 2024, Orlando, USA. Paper number AIAA 2024-2875
DOI:10.2514/6.2024-2875

Dynamics Modeling of Multirotor type UAV with the Blade Element Momentum Theory and Nonlinear Controller Design for a Wind Environment

On Park* and Hyo-Sang Shin.†
Cranfield University, Bedfordshire, MK43 0AL, United Kingdom

This paper presents an aerodynamics modeling of a rotary type Vertical Take-Off and Landing (VTOL) aircraft using the Blade Element Momentum Theory (BEMT). The BEMT is incorporated into the rigid body dynamics to describe main force and its reactive torque by rotor of the multirotor UAV. The dynamics modeling can demonstrate the motion of the multirotor UAV in the presence of gust or wind in an unsteady environment effectively. In order to operate the multirotor UAV, a robust nonlinear control technique is designed to track the desired command and stabilize the UAV subject to uncertainties such as modeling error, external disturbances. The hierarchical Sliding Mode Control (SMC) is adopted to organize a multi-loop structure: the outer-loop and inner-loop mode. Actual control input is distributed by physical configuration of the multirotor UAV with the described thrust and torque modeling by the BEMT in the control allocation. Numerical simulation evaluates the feasibility of the dynamic modeling of the multrirotor UAV with BEMT in the presence of external wind effects, which enables to understand a motion of rotary type UAV in a windy environment.

Nomenclature

$\mathbf{v}^b$	=	velocity in the body frame
$\boldsymbol{\omega}^b$	=	angular velocity in the body frame
$\mathbf{v}^I$	=	velocity in the inertial frame
$\mathbf{v}_r^b$	=	total velocity in the body frame
$\boldsymbol{\omega}_r^b$	=	total angular velocity in the body frame
v_r^I	=	total velocity in the inertial frame
$\mathbf{q}$	=	quaternion
Φ	=	Euler angle
α, β	=	angle of attack, angle of side slip
$F^b_{(x,y,z)}$	=	resultant forces acting on the body frame
$M^b_{(x,y,z)}$	=	resultant moments acting on the body frame
$C_{\{T,H,Q\}}$	=	aerodynamic coefficient of thrust, horizontal force, and torque
N	=	number of blade
c, b, R, A	=	chord length of blade airfoil, blade span, disc radius, disc area
μ, λ	=	advanced ratio, rotor infow ratio
j	=	rotor index
Ω_j, l_j	=	jth rotor speed, jth rotor position
m, J_b	=	mass, moment of inertia
$\mathbf{R}_a^b$	=	coordinate transformation matrix from a frame to b frame
ρ	=	air density

I. Introduction

Unmanned Aerial Vehicle (UAV) is getting more and more attention and its demand for civil area has been increased over the last decade. Especially, rotary type UAV such as quadrotor or this kind of multirotor type UAV is widely

*Research Fellow, School of Aerospace, Transport and Manufacturing (SATM), Cranfield University, O.Park@cranfield.ac.uk
†Professor, School of Aerospace, Transport and Manufacturing (SATM), Cranfield University, h.shin@cranfield.ac.uk

Published by AIAA. This is the Author Accepted Manuscript issued with: Creative Commons Attribution License (CC:BY 4.0).
The final published version (version of record) is available online at DOI:10.2514/6.2024-2875. Please refer to any applicable publisher terms of use.

used, since it is easy to operate, light, inexpensive and its capabilities to the Vertical Take-Off and Landing (VTOL), hovering and maneuvering enable to be used in various missions. However, external disturbances can significantly affect on the multirotor UAV, because most multirotor UAV is vulnerable to the disturbances due to less mass, inertia and thrust power compared to the conventional aircraft [1, 2]. For this reason, the understanding for the multirotor manuevering is important to the engineers to operate the UAV effectively. In the past, most of the researches on the multirotor consider a simple kinematics relation by Newton-Lagrangian method with static thrust forces generated by rotors, however, this assumption is not valid to understand the multirotor behaviour in the windy environment or external disturbances. Hence, the studies on the aerodynamics characteristics of the multirotor body and rotating propeller are carried out via wind tunnel tests [3] and Computational Fluid Dynamics (CFD) [4]. In addition, the mathematical modeling of the rotating propeller is developed by utilizing the established rotorcraft dynamics [5–8].

Various control methods have been designed to operate multirotor UAV for trajectory tracking problem or stabilizing its attitudes. Classic linear controller, Proportional-Integrator-Derivative (PID) controller, Linear Quadratic (LQ) controller [8, 9], and nonlinear controller, backstepping control, nonliner dynamic inversion [1, 10, 11], are implemented in the multirotor UAV control problem. Among them, Sliding Mode Control (SMC) that is one of robust control methods is a promising approach to deal with uncertainties acting on the multirotor UAV flight such as implicit system fault, external wind and disturbances in a practical application. As an alternative, uncertainty estimator can be incorporated, for example by using Sliding Mode Disturbance Observer (SMDO) to handle estimation error by SMC [12, 13].

In this paper, the multirotor dyanmics modeling based on the helicopter dynamics [14, 15] is developed to demonstrate multirotor maneuvering in an unsteady environment taking into account external disturbances. The standard six Degree of Freedom (6DOF) dynamics is modeled by Newton's 2nd law and the air surrounding dynamics is derived considering the relative wind effect from initially referenced dynamics. The Blade Element Momentum Theory (BEMT) incorporating blade lelement theory and momentum theory is utilized on the thrust force modeling to investigate aerodynamic forces and moments acting on the multirotor UAV [6, 8]. The conventional SMC is then designed by utilizing a cascaded control structure: position and attitude loops. Each loop has a its rate feedback in the inner loop to design a Stability and Controllability Augmentation System (SCAS) structure. Indeed, the control mapping of the actual input from the force and moment given by attitude controller is represented with the aerodynamic coefficient based on the BEMT.

The rest of this paper is organized as follows: Section II describes the equation of motion for the rigid body dynamics. The BEMT is introduced to demonstrate the aerodynamic forces and moments generated by a rotor, and the multirotor UAV is modelled incorporated the rigid body dynamics with the BEMT. In Section III, Robust controller is designed as a baseline controller. The cascaded SMC for position tracking loop and stabilizing attitude loop is designed based on the command error and the control mapping is designed by the BEMT. Section IV shows the numerical simulation result validating the developed dynamics and controller. Finally, a conclusion is given in Section V.

II. Multirotor Dynamics Modeling

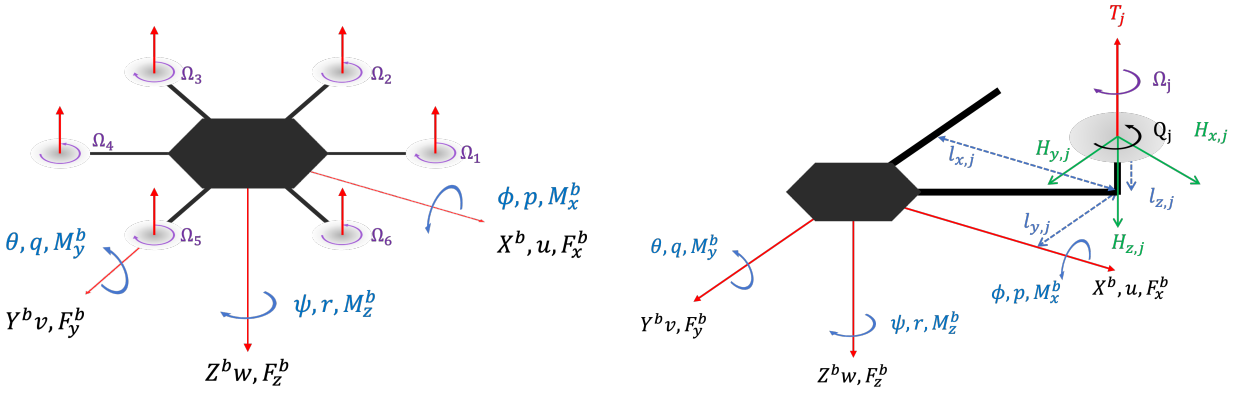
A. Equation of Motion for rigid body dynamics

The motion of multirotor shown in the Fig.1 can be derived by Newton's law with a rigid body assumption [16, 17]:

$$\begin{aligned} \dot{\mathbf{v}}^b &= \frac{F^b_{tot}}{m} - \boldsymbol{\omega}^b \times \mathbf{v}^b \\ \dot{\boldsymbol{\omega}}^b &= J_b^{-1}(M^b_{tot} - \boldsymbol{\omega}^b \times J_b \boldsymbol{\omega}^b) \end{aligned} \tag{1}$$

where $\mathbf{v}^b = [u, v, w]^T$ and $\boldsymbol{\omega}^b = [p, q, r]^T$ are velocity and angular velocity of the multirotor and $F^b_{tot} = [F_x, F_y, F_z]^T$ and $M^b_{tot} = [M_x, M_y, M_z]^T$ denote the total external forces and moments applied on the multirotor with respect to its body frame with the mass m and inertia matrix J_b given by

$$J_b = \begin{bmatrix} I_{xx} & 0 & -I_{xz} \\ 0 & I_{yy} & 0 \\ -I_{zx} & 0 & I_{zz} \end{bmatrix} \tag{2}$$



(a) System configuration of multirotor UAV **(b) Geometry of multirotor model**

Fig. 1 Overview of multirotor model

The rotational kinematics of the multirotor is represented by the quaternion $\mathbf{q} = [q_0, q_1, q_2, q_3]^T$ to prevent the singularity issue

$$\dot{\mathbf{q}} = \frac{1}{2}\begin{bmatrix} 0 & -p & -q & -r \\ p & 0 & r & -q \\ q & -r & 0 & p \\ r & q & -p & 0 \end{bmatrix}\mathbf{q} \tag{3}$$

and its angular attitude or Euler angles $\Phi = [\phi, \theta, \psi]^T$ are the roll, $\phi \in [-\frac{\pi}{2}\ \frac{\pi}{2}]$, the pitch, $\theta \in [-\frac{\pi}{2}\ \frac{\pi}{2}]$ and the yaw $\psi \in [-\pi\ \pi]$ that can be obtained from the quaternion. The velocity of multirotor defined in the North-East-Down (NED) position relative to the inertial frame is transformed from the $\mathbf{v}^b$ as:

$$\mathbf{v}^I = \mathbf{R}_b^I \mathbf{v}^b \tag{4}$$

where $\mathbf{v}^I = [v_n, v_e, v_d]^T$ is the velocity components in terms of the inertial frame or NED frame and $\mathbf{R}_b^I$ is the rotation matrix that transforms a vector from the body frame to inertial frame:

$$\begin{aligned} \mathbf{R}_b^I &= \begin{bmatrix} \cos\psi & \sin\psi & 0 \\ -\sin\psi & \cos\psi & 0 \\ 0 & 0 & 1 \end{bmatrix}^T \begin{bmatrix} \cos\theta & 0 & -\sin\theta \\ 0 & 1 & 0 \\ \sin\theta & 0 & \cos\theta \end{bmatrix}^T \begin{bmatrix} 1 & 0 & 0 \\ 0 & \cos\phi & \sin\phi \\ 0 & -\sin\phi & \cos\phi \end{bmatrix}^T \\ &= \mathbf{R}_z^T(\psi)\mathbf{R}_y^T(\theta)\mathbf{R}_x^T(\phi) \end{aligned} \tag{5}$$

where the $\mathbf{R}(\cdot)$ is a rotating matrix through an Euler angle $\Phi = [\phi, \theta, \psi]^T$.

B. Blade Element Momentum Theory

Each motors generates an upward thrust force by rotating propellers, which is the main manoeuvering forces and moments. In order to express a thrust force and moment, the BEMT is applied to analyze how an aerodynamics forces and moments effect on the multirotor. This subsection summarizes the BEMT briefly to derive the aerodynamic force and moments by a rotor. First, the configuration of the propeller is shown in Fig. 2. The forces and torque of rotor are can be given by momentum theory of rotors [14, 15]:

$$\begin{aligned} T &= \rho A(\Omega R)^2 C_T \\ H &= \rho A(\Omega R)^2 C_H \\ Q &= \rho A(\Omega R)^2 R C_Q \end{aligned} \tag{6}$$

where T, H, Q are the thrust, horizontal force and reactive toque of the motor, respectively. ρ is the air density, A is area of the rotating propeller plane, Ω is the rotor speed, R is the propeller radius, and $C_{\{\cdot\}}$ are its force and torque

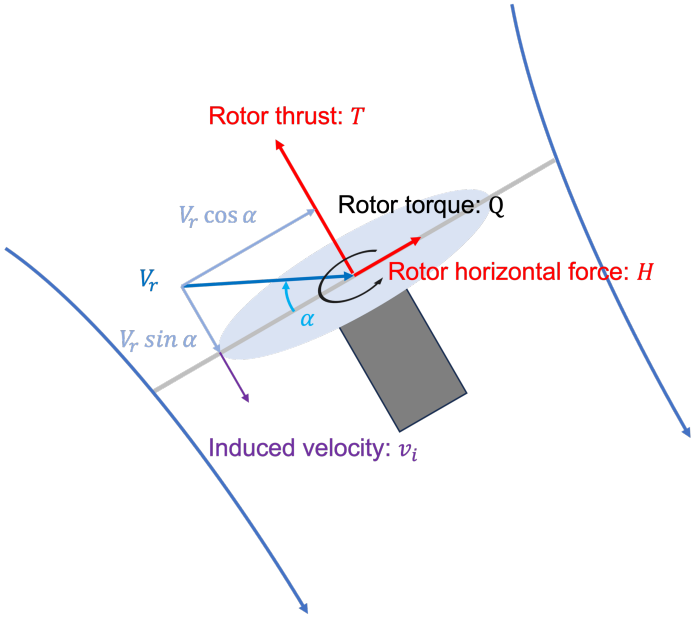


Fig. 2 Momentum theory of air flow model

coefficients which can be calculated by blade element theory [8, 14]:

$$
\begin{aligned}
C_T &= \frac{1}{2}\sigma C_L\left(\frac{1}{3}\theta'(1+\frac{3}{2}\mu^2)-\frac{1}{2}\lambda-\frac{1}{2}\mu a_1\right)\\
C_H &= \frac{C_L\sigma}{2}\left[\frac{\mu C_{D_0}}{2C_L}+\frac{1}{3}a_1\theta'-\frac{3}{4}\lambda a_1+\frac{1}{2}\mu\theta'\lambda+\frac{1}{4}\mu a_1^2\right]\\
C_Q &= \frac{\sigma}{4}\left[\frac{C_{D_0}}{2}(1+\mu^2)+\frac{C_{D_\alpha}}{1+3/2\mu^2}\left\{\theta_0'\left(\frac{1}{2}-\frac{19}{36}\mu^2+\frac{3}{4}\mu^4\right)+\theta_1'\left(\frac{2}{5}(1-\mu^2)+\frac{1}{2}\mu^4\right)+\frac{1}{3}\lambda(2-\mu^2)\right\}\right]
\end{aligned}
\tag{7}
$$

where $\sigma = Nc/(\pi R)$ is the ratio of the rotor blade area (NcR) to the total rotor disk area (πR^2) shown in the Fig. 3. C_L

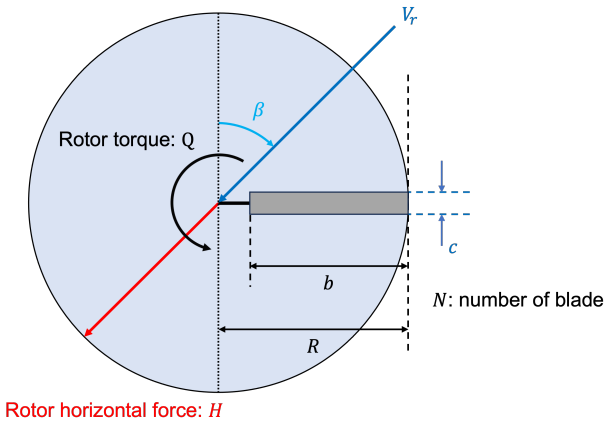


Fig. 3 Top view of the rotor disc

is the propeller lift coefficient, C_{D_0} and C_{D_α} are the drag coefficients, $\theta' = \theta_0' + \frac{3}{4}\theta_1'$ is the blade pitch angle with the blade pitch θ_0' at the root and twist θ_1'. A tip speed ratio or advanced ratio μ is the ratio of the relative air velocity to the

tip speed of its rotor as follows:

$$\mu = \frac{V_a \cos\alpha}{\Omega R} \tag{8}$$

where V_a is the velocity referenced to the air surrounding the multirotor, (or airspeed), α is the angle of attack between the and the blade section. The rotor inflow ratio, λ, is the ratio of total inflow velocity to rotor tip speed:

$$\lambda = \frac{V_a \sin\alpha + v_i}{\Omega R} \tag{9}$$

where v_i is the induced velocity calculated by solving the following equation:

$$\left(\frac{v_i}{v_h}\right)^4 + \left(\frac{V_a}{v_h}\right)^2 \left(\frac{v_i}{v_h}\right)^2 = 1 \tag{10}$$

with the induced velocity in hover $v_h^2 = T/(2\rho A)$. The backward flapping angle a_1 is

$$a_1 = \frac{\mu(8/3\theta_0' - 2\lambda)}{1 - 1/2\mu^2} \tag{11}$$

C. External Forces and Moments by BEMT

The fundamental BEMT for the aerodynamics of rotating propeller is described in the subsection II.B. The external forces and moments in Eq. (1) are mainly derived by the thrust and horizontal force T, H and torque Q from the rotor, which is obtained by the surrounding air. Hence, it is essential to distinguish the airspeed by the velocity with respect to the surrounding air [17], which can be defined as:

$$\begin{aligned} \mathbf{v}_r^b &= \mathbf{v}^b - \mathbf{v}_w^b \\ \boldsymbol{\omega}_r^b &= \boldsymbol{\omega}^b + \boldsymbol{\omega}_w^b \\ \mathbf{v}_r^I &= \mathbf{R}_b^I \mathbf{v}_r^b + \mathbf{v}_w^I \end{aligned} \tag{12}$$

where $\mathbf{v}_w^b = \mathbf{R}_I^b \mathbf{v}_w^I$ and $\boldsymbol{\omega}_w^b = \mathbf{R}_I^b \omega_w^I$ are the wind velocity and angular velocity in the body frame, and $\mathbf{v}_r^b$ and ω_r^b are the body components of the relative airspeed and angular velocity vectors, respectively and $\mathbf{v}_r^I$ is the relative velocity in terms of the inertial frame. The magnitude, Angle of Attack (AoA) and Angle of Sideslip (AoS) of the multirotor can then be calculated by:

$$\begin{aligned} V_a &= |\mathbf{v}_r^b|_2 \\ \alpha &= \tan^{-1}(w_r/u_r) \text{ or } \sin^{-1}(w_r/V_a) \\ \beta &= \sin^{-1}(v_r/V_a) \end{aligned} \tag{13}$$

In addition, actual velocity ($\mathbf{v}_{r,j}^b$) and its angle of attack (α_j) and sideslip angle(β_j) of each rotors relative to the center of mass are expressed by:

$$\begin{aligned} \mathbf{v}_{r,j}^b &= \mathbf{v}_r^b + (\boldsymbol{\omega}_r^b \times l_j) \\ V_{a,j} &= |\mathbf{v}_{r,j}^b|_2 \\ \alpha_j &= \tan^{-1}(w_{r,j}/u_{r,j}) \\ \beta_j &= \sin^{-1}(v_{r,j}/V_{a,j}) \end{aligned} \tag{14}$$

where the subscript, j, denotes the motor number shown in Fig. 1 and $l_j = [l_{x,j}, l_{y,j}, l_{z,j}]^T$ is the position of the motor measured from the center of mass. Hence, the actual velocity, angle of attack and side slip angle $[V_{a,j}, \alpha_j, \beta_j]$ for each rotor replace $[V_a, \alpha, \beta]$ in Eq.(8) - Eq.(10). The resultant forces acting on the multirotor can then be calculated by

$$\begin{aligned} F_{tot}^b &= F_T^b + F_H^b + F_g^b \\ M_{tot}^b &= M_T^b + M_H^b + M_Q^b \end{aligned} \tag{15}$$

The following control mapping relation (or control allocation matrix) is satisfied by the configuration of the multirotor shown in the Fig. 1.

$$\begin{bmatrix} F_T^b \\ M_x^b \\ M_y^b \\ M_z^b \end{bmatrix} = M_{CA} \begin{bmatrix} \Omega_1^2 \\ \Omega_2^2 \\ \Omega_3^2 \\ \Omega_4^2 \\ \Omega_5^2 \\ \Omega_6^2 \end{bmatrix} \tag{16}$$

where component of the control allocation matrix can be derived as:

$$\begin{aligned} M_{CA}(1,j) &= -(\bar{C}_{T_j} - \bar{C}_{H_{z,j}}) \\ M_{CA}(2,j) &= -(\bar{C}_{T_j} - \bar{C}_{H_{z,j}}) l_{y,j} \\ M_{CA}(3,j) &= (\bar{C}_{T_j} - \bar{C}_{H_{z,j}}) l_{x,j} \\ M_{CA}(4,j) &= -\bar{C}_{H_{x,j}} l_{y,j} + \bar{C}_{H_{y,j}} l_{x,j} + (-1)^j \bar{C}_{Q_j} \end{aligned} \tag{17}$$

where $\bar{C}_{T_j} = \rho A R^2 C_{T_j}$, $\bar{C}_{H_j} = \rho A R^2 C_{H_j}$, $\bar{C}_{Q_j} = \rho A R^2 C_{Q_j} R$ are introduced from the Eq.(6). The horizontal force F_H and the gravitational force F_g are decomposed into body frame components corresponding to its axis by:

$$F_H^b = \begin{bmatrix} H_{x,j} \\ H_{y,j} \\ H_{z,j} \end{bmatrix} \tag{18}$$

$$F_g^b = \mathbf{R}_I^b \begin{bmatrix} 0 \\ 0 \\ g \end{bmatrix} \tag{19}$$

where $\mathbf{R}_I^b = \mathbf{R}_1(\phi)\mathbf{R}_2(\theta)\mathbf{R}_3(\psi)$ is the transformation matrix from inertial frame to body frame.

III. Controller Design

A. Sliding Mode Control

In this section, the SMC is designed for the multirotor manoeuver in the presence of dynamics uncertainties or external disturbances [18]. The Fig. (4) shows the cascaded SMC structure where the outer loop is designed for the command tracking while the inner loop stabilizes its state variables. Each of cascaded inner and outer loop controllers is designed based on the PI sliding surface concept. The designed sliding surface and stability analysis guarantee the convergence property by the Lyapunov theory.

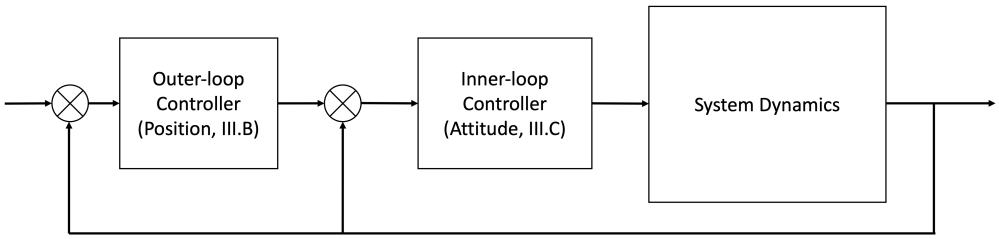


Fig. 4 Cascaded Controller Structure

Consider the following nonlinear dynamics as follows:

$$\dot{x} = f(x) + g(x)u + d \tag{20}$$

where x is the system state, $f(x)$ and $g(x)$ are the known nonlinear system dynamics u is the control input, and $|d| \leq D$ is the uncertainty or disturbance. Define the following sliding surface in the PI controller form as:

$$S = K_P e + K_I \int_0^t e d\tau \tag{21}$$

where $e = x - x_c$ and $\dot{e}$ are the tracking error and its derivative with the PI gain, K_P, K_I. The time derivative of the sliding surface Eq.(21) is

$$\begin{aligned} \dot{S} =& K_P \dot{e} + K_I e \\ =& K_P(\dot{x} - \dot{x}_c) + K_I e \end{aligned} \tag{22}$$

Consider the Lyapunov candidate function:

$$V = \frac{1}{2} S^T S \tag{23}$$

Taking the time derivative of Eq.(23)

$$\begin{aligned} \dot{V} =& S^T \dot{S} \\ =& S^T [K_P \dot{e} + K_I e] \\ =& S^T [K_P(\dot{x} - \dot{x}_c) + K_I e] \\ =& S^T [K_P\{f(x) + g(x)u + d - \dot{x}_c\} + K_I e] \end{aligned} \tag{24}$$

Make sure the time derivative of the Lyapunov candidate function, $\dot{V} \leq 0$, the following control input can be derived

$$u = g^{-1}(x)[-f(x) + \dot{x}_c - K_P^{-1}\{K_I e + C_1 S + C_2 \text{sgn}(S)\}] \tag{25}$$

where C_1 is a positive definite diagonal matrix and $|D| \leq C_2$. However, the one of the difficulties in the SMC approach is a chattering issue caused by discontinuity of the $sig(S)$ function. In order to mitigate un undesirable response, the following function replaces $sgn(S)$ in the Eq.(25):

$$sat(S) = \begin{cases} S/\epsilon & \text{if } |s/\epsilon| \leq 1 \\ sgn(S/\epsilon) & \text{otherwise} \end{cases} \tag{26}$$

where $\epsilon > 0$. Substituting the derived control input Eq.(25) into the Eq.(24) yields

$$\begin{aligned} \dot{V} &= S^T d - C_1 S^T S - C_2 |S| \\ &\leq |d^T S| - C_1 S^T S - C_2 |S| \\ &\leq |D||S| - C_1 S^T S - C_2 |S| \\ &\leq -C_1 S^T S - (C_2 - |D|)|S| \\ &\leq 0 \end{aligned} \tag{27}$$

Therefore, the sliding surface S converges to zero as t tends to ∞ asymptotically by Lyapunov stability criterion.

B. Position Control

In this subsection, the position controller is designed for multirotor position tracking subjected to external disturbances. The main objective is to track the target position the desired way point, $x_c = [N_c, E_c, D_c]^T$, utilizing a following

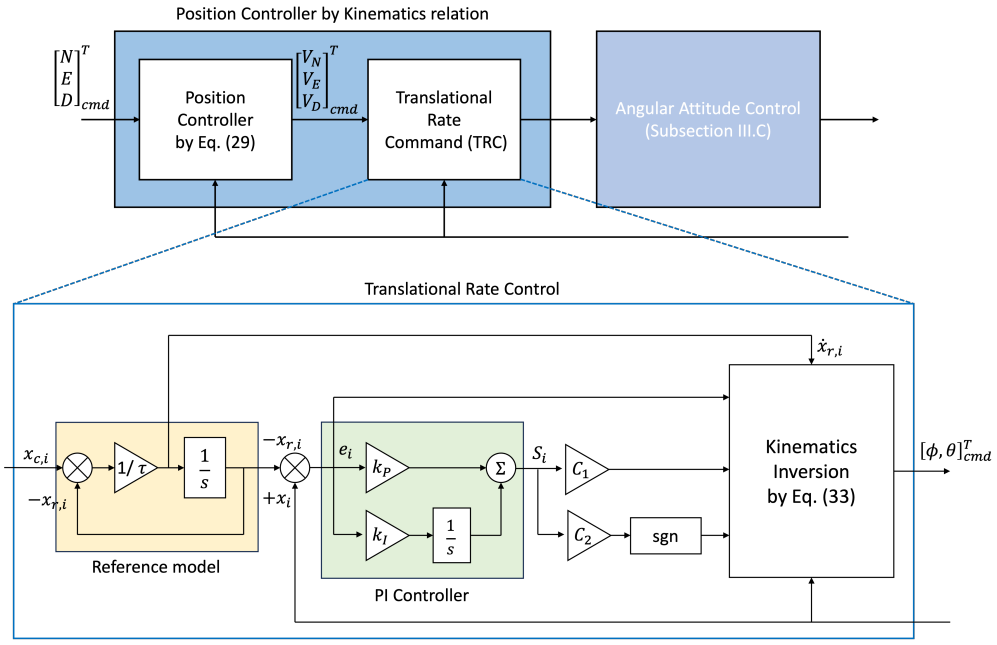


Fig. 5 SMC: Translational Rate Control

kinematic model for NED coordinate instead of the navigation equation, Eq. (4), as follows:

$$\begin{aligned}\frac{d^2}{dt^2}\begin{bmatrix}N\\E\\D\end{bmatrix} &= \frac{1}{m}\mathbf{R}_z^T(\psi)\mathbf{R}_y^T(\theta)\mathbf{R}_x^T(\phi)\mathbf{F}_{tot}^b \\ &= \frac{1}{m}\mathbf{R}_z^T(\psi)\mathbf{R}_y^T(\theta)\mathbf{R}_x^T(\phi)\begin{bmatrix}0\\0\\F_T^b + F_g^b\end{bmatrix} \\ &= \frac{d}{dt}\begin{bmatrix}V_N\\V_E\\V_D\end{bmatrix}\end{aligned} \tag{28}$$

where $F_T = -\sum T_j$ is the total thrust force generated by each rotor j. The acceleration, $[\ddot{N}, \ddot{E}, \ddot{D}]^T$ can be considered as a time derivative of ground velocity, $[\dot{V}_N, \dot{V}_E, \dot{V}_D]$, hence position controller can be divided into inner and outer loops by position and velocity loops. The position loop consists of a simple linear controller, i.e. PID controller as:

$$V_{cmd} = K_P e_{pos} + K_I \int e_{pos} d\tau + K_D \dot{e}_{pos} \tag{29}$$

where $e_{pos} = [N, E, D]^T_{cmd} - [N, E, D]^T$ and $K_{(P,I,D)}$ are position error and its PID gains, respectively. The velocity loop can utilise Eq. (28) to formulate in Eq. (20), the control input can then be found with mathematical manipulations, which is called as a Translational Rate Control, (TRC) mode shown in Fig. 5 [19]. In order to derive an angular attitude command, $[\phi, \theta]^T_{cmd}$, kinematic inversion relation is adopted with a virtual control input, ν as:

$$\begin{aligned}\frac{d}{dt}\begin{bmatrix}V_N\\V_E\\V_D\end{bmatrix} &= \begin{bmatrix}0\\0\\g\end{bmatrix} + \frac{1}{m}\mathbf{R}_z^T(\psi)\mathbf{R}_y^T(\theta)\mathbf{R}_x^T(\phi)\begin{bmatrix}0\\0\\F_T^b\end{bmatrix} \\ &= \nu\end{aligned} \tag{30}$$

By applying Eq. (30) into Eq. (20) and Eq. (21) yields a virtual input (ν) as:

$$\nu = \dot{x}_c - K_P^{-1}[K_I e + C_1 S + C_2 \text{sgn}(S)] \tag{31}$$

Expanding this matrix equations results in:

$$\begin{aligned} \underbrace{m\mathbf{R}_z(\psi)\left(\nu - \begin{bmatrix}0\\0\\g\end{bmatrix}\right)}_{=\nu'} &= \mathbf{R}_y^T(\theta)\mathbf{R}_x^T(\phi)\begin{bmatrix}0\\0\\F_T^b\end{bmatrix} \\ &= \begin{bmatrix}F_T^b\cos\phi\sin\theta\\ -F_T^b\sin\phi\\ F_T^b\cos\phi\cos\theta\end{bmatrix} \end{aligned} \tag{32}$$

Solving for Euler angle command $[\phi, \theta]_{cmd}^T$ utilizing kinematics inversion yields:

$$\begin{aligned} \sin\phi_c &= -\frac{1}{F_T^b}\nu'(2) \\ \tan\theta_c &= \frac{\nu'(1)}{\nu'(3)} \end{aligned} \tag{33}$$

where F_T^b is calculated by

$$F_T^b = m\left\|\begin{matrix}\dot{V}_N\\ \dot{V}_E\\ \dot{V}_D - g\end{matrix}\right\|_2 = m\left\|\begin{matrix}\nu(1)\\ \nu(2)\\ \nu(3) - g\end{matrix}\right\|_2 \tag{34}$$

C. Attitude Control

Similar to the position loop controller, the inner loop controller can be derived to stabilize its angular attitude performing the desired position tracking. Consider the following affine system dynamics as:

$$\dot{x}_i = f_i(x) + g_i(x)u_i + d_i \tag{35}$$

Instead of the quaternion equation used for the angular attitude in the dynamics by Eq.(3), the stabilization of angular attitude, i.e. rotational kinematics relation with Euler angle, $\Phi = [\phi, \theta, \psi]^T$, is adopted:

$$\frac{d}{dt}\begin{bmatrix}\phi\\\theta\\\psi\end{bmatrix} = \begin{bmatrix}1 & \sin\phi\tan\theta & \cos\phi\tan\theta\\ 0 & \cos\phi & -\sin\phi\\ 0 & \sin\phi/\cos\theta & \cos\phi/\cos\theta\end{bmatrix}\begin{bmatrix}p\\q\\r\end{bmatrix} \tag{36}$$

Recall and reformulate the moment equation in Eq. (1) for angular rate control as follows:

$$\begin{aligned} \dot{\boldsymbol{\omega}}^b &= J_b^{-1}(M_{tot} - \boldsymbol{\omega}^b \times J_b\boldsymbol{\omega}^b) \\ &= -J_b^{-1}(\boldsymbol{\omega}^b \times J_b\boldsymbol{\omega}^b) + J_b^{-1}M_{tot} \end{aligned} \tag{37}$$

where Eq. (35) can be defined by cascaded structure with the $x_1 = \Phi = [\phi, \theta, \psi]^T$ and $u_1 = \boldsymbol{\omega}^b = [p, q, r]^T$ for outer loop and $x_2 = \boldsymbol{\omega}^b = [p, q, r]^T$ and $u_2 = \mathbf{M}_{tot}^b = [M_x^b, M_y^b, M_z^b]^T$ for inner loop, respectively. Thus, the affine system model for cascaded structure of angular attitude loop illustrated in Fig. 6 can be defined as:

$$\begin{aligned} f_1(x) &= 0_{3\times1} \\ g_1(x) &= \begin{bmatrix}1 & \sin\phi\tan\theta & \cos\phi\tan\theta\\ 0 & \cos\phi & -\sin\phi\\ 0 & \sin\phi/\cos\theta & \cos\phi/\cos\theta\end{bmatrix} \\ f_2(x) &= -J_b^{-1}(\boldsymbol{\omega}^b \times J_b\boldsymbol{\omega}^b) \\ g_2(x) &= J_b^{-1} \end{aligned} \tag{38}$$

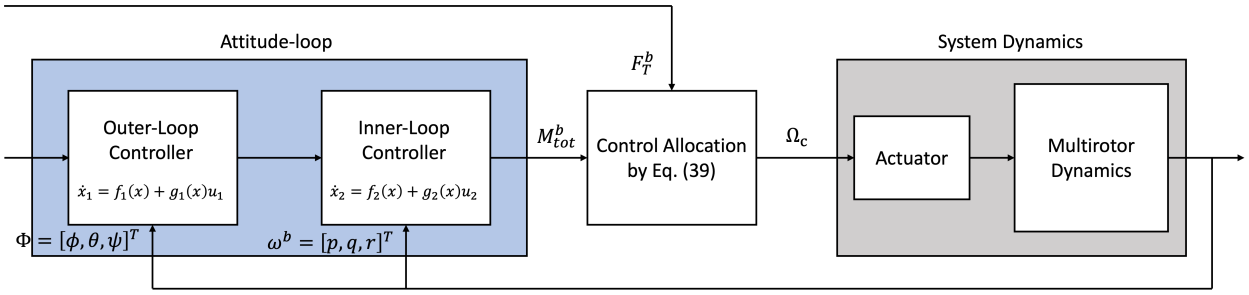


Fig. 6 SMC: angular attitude control

Lastly, The commanded pseudo control input, $\nu_{FM} = [F_T^b, M_x^b, M_y^b, M_z^b]^T$ from the TRC of position loop by Eq. (34) and moments by $u_2 = M_{tot}^b$ of angular attitude loop, is then distributed to the actual motor speed Ω by geometric configuration of multirotor with control mapping relation by Eq. (16) and (17).

$$\Omega = M_{CA}^{\dagger} \nu_{FM} \tag{39}$$

where $M_{CA}^{\dagger}$ is a pseudo inverse matrix obtained by solving an optimized-based control allocation problem [11].

IV. Numerical Simulation

In this section, the numerical simulation is carried out to validate the multirotor modeling with the rigid body dynamics and the BEMT. The multirotor UAV considered in this section is Draganflyer X-Pro of which parameters and data sheet are provided by [8, 20]. The cascaded SMC structure and the dynamics with the BEMT are shown in Fig. 7 and the spatial wind data modelled by the CFD is provided from [21]. The reference command is transferred to the

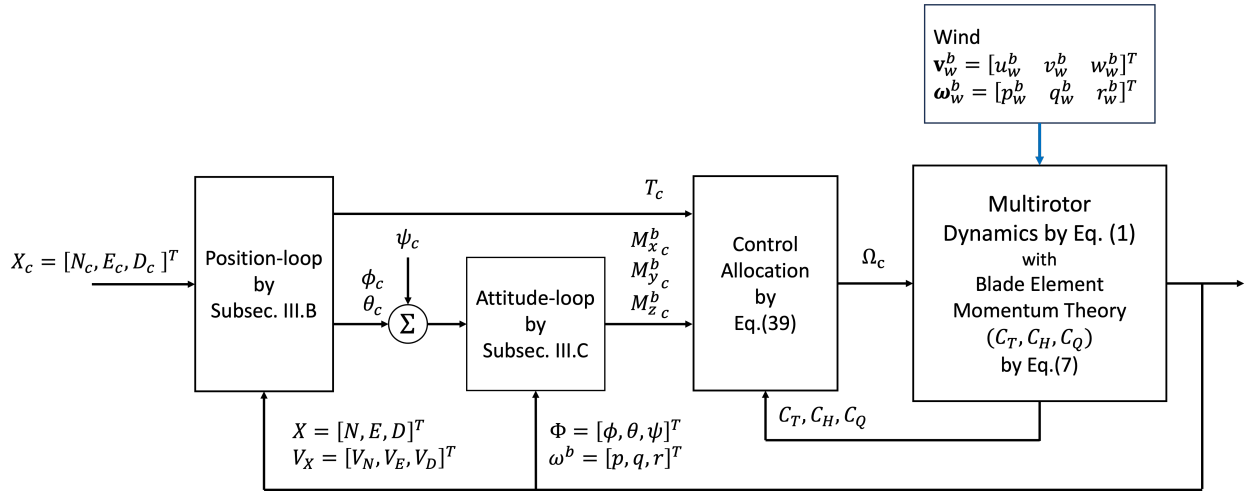


Fig. 7 Overview of Control structure

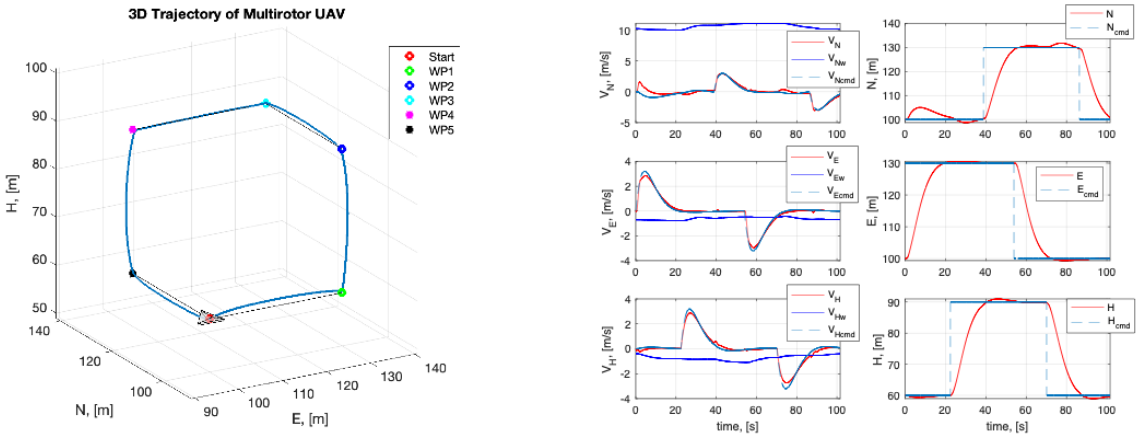
TRC-loop through the following 1*st*-order command filter to obtain the $\dot{x}_r$:

$$\frac{x_r(s)}{x_c(s)} = \frac{1}{\tau s + 1} \tag{40}$$

where the time constant is set by $\tau = 3$ [19]. The filtered command x_r and its derivatives replace the x_c and $\dot{x}_c$ in Eq. (21). The controller gains and its parameters are presented in Table 1. Fig. 8 shows the result of waypoint tracking guidance in a windy environment. Fig. 8a illustrates the 3D trajectory of the flight mission and the detailed trajectories are given in Fig 8b. The solid red line means the actual response of state variable, solid blue line represents the external wind and the dashed line indicates the command for corresponding variable. Here, the vertical motion of the NED

Table 1 SMC gains and parameters

Gain parameter		value	Gain parameter		value
Position	$K_{P_{(N,E,D)}}$	$[0.4, 0.4, 0.4]$	Velocity	$K_{P_{(V_N,V_E,V_D)}}$	$[5, 5, 5]$
	$K_{I_{(N,E,D)}}$	$[0, 0, 0]$		$K_{I_{(V_N,V_E,V_D)}}$	$[0.1, 0.1, 0.1]$
	$K_{D_{(N,E,D)}}$	$[0.4, 0.4, 0.4]$		$C1_{(V_N,V_E,V_D)}$	$[1, 1, 1]$
	-	-		$C2_{(V_N,V_E,V_D)}$	$[1, 1, 1]$
	-	-		$\epsilon_{(V_N,V_E,V_D)}$	$[5, 5, 5]$
Euler angle	$K_{P_{(\phi,\theta,\psi)}}$	$[1, 1, 1]$	Angular rate	$K_{P_{(p,q,r)}}$	$[1, 1, 1]$
	$K_{I_{(\phi,\theta,\psi)}}$	$[0, 0, 0]$		$K_{I_{(p,q,r)}}$	$[0, 0, 0]$
	$C1_{(\phi,\theta,\psi)}$	$[0, 0, 0]$		$C1_{(p,q,r)}$	$[0, 0, 0]$
	$C2_{(\phi,\theta,\psi)}$	$[1, 1, 1]$		$C2_{(p,q,r)}$	$[1, 1, 1]$
	$\epsilon_{(\phi,\theta,\psi)}$	$[0.5, 0.5, 0.5]$		$\epsilon_{(p,q,r)}$	$[0.5, 0.5, 0.5]$



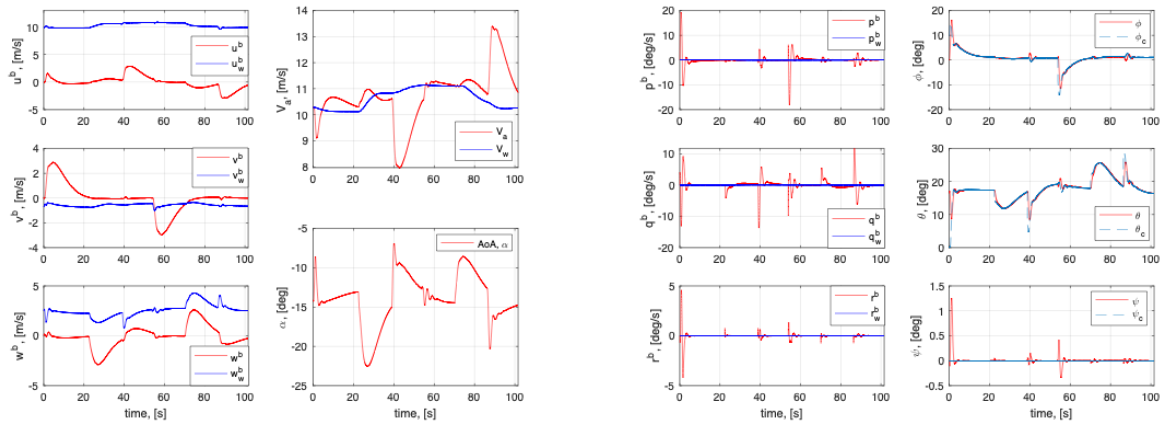
(a) 3D trajectory of flight **(b) Time history of NED coordinate variables**

Fig. 8 Result of the way point tracking simulation: navigation variables

coordinate is illustrated by Height, H, by $H = -D$ or $V_H = -V_D$. As shown in the left side of the Fig. 8b, spatial wind profiles exist during the simulation, which is not a constant wind but a variant wind. The Fig. 9 shows the time history of responses: translational velocity in terms of body-fixed framework, AoA in Fig. 9a and rotational velocity and Euler angle in Fig. 9b. The magnitudes of wind profile $(\mathbf{v}_w^I, \boldsymbol{\omega}_w^b)$ are less than the parameter for the sign function in the control input in Eq. (25) set in the Table 1, hence the validity of the SMC parameter, especially, C_2 is confirmed by Eq. (27). The maximum values of each SMC loop, i.e. $[V_{(N,E,D)}, \Phi, \boldsymbol{\omega}^b]$, are less than ϵ set in the Table 1, the *sat* function in Eq. (26) is also validated. When it comes to the angular attitude (Euler angle), the its attitude is tilted to hover and manoeuver against the wind environment, especially roll and pitch angle shown in Fig. 9b due to the wind profile u_w^b and v_w^b. And an aerodynamic angle, AoA, can also consider an external wind effect shown in Fig. 9a, which takes into account the rotor coefficient. Thus, the BEMT-based multirotor modeling built in the subsection II.B and II.C can express the equation of motion in the windy environment or external disturbance effects.

V. Conclusion

In this paper, the dynamics modeling for the rotary type UAV is investigated. The 6DOF rigid body dynamics is derived and the rotor thrust and moment acting on the multirotor are modelled based on the rotorcraft dynamics using the BEMT. The proposed dynamics modeling in the body fixed frame at the center of gravity distinguishes the equation of motion in the inertial frame by coordinate transform, which can provide a proper relation.



(a) Time history of translational state variables **(b) Time history of rotational state variables**

Fig. 9 Result of the way point tracking simulation: body-fixed coordinate responses

Based on the derived dynamics modeling with the BEMT, the nonlinear controller is designed by SMC technique for the operation in an uncertain environment. The designed control loop is made up of cascaded structure: a position control system in the outer loop and attitude control in the inner loop. The separated position control is addressed by adopting TRC mode, which enables to utilize an affine system form by incorporate velocity feedback loop into the position control, and the attitude controller is designed by utilizing a conventional stability and controllabilty augmentation system structure. The actual control input is then derived by solving new control mapping configuration based on the BEMT modeling. The numerical simulation validates the BEMT-based multirotor modeling considering an external wind effect.

Acknowledgments

The authors would like to acknowledge support from UKRI Innovate UK under the "SafeZone phase3" project under 10025740 under the Future Flight programme.

References

[1] Bouabdallah, S., and Siegwart, R., "Backstepping and sliding-mode techniques applied to an indoor micro quadrotor," *Proceedings of the 2005 IEEE international conference on robotics and automation*, IEEE, 2005, pp. 2247–2252.

[2] Wang, H., Ye, X., Tian, Y., Zheng, G., and Christov, N., "Model-free–based terminal SMC of quadrotor attitude and position," *IEEE Transactions on Aerospace and Electronic Systems*, Vol. 52, No. 5, 2016, pp. 2519–2528.

[3] MacNeill, R., and Verstraete, D., "Blade element momentum theory extended to model low Reynolds number propeller performance," *The Aeronautical Journal*, Vol. 121, No. 1240, 2017, pp. 835–857.

[4] Ventura Diaz, P., and Yoon, S., "High-fidelity computational aerodynamics of multi-rotor unmanned aerial vehicles," *2018 AIAA Aerospace Sciences Meeting*, 2018, p. 1266.

[5] Orsag, M., and Bogdan, S., "Influence of forward and descent flight on quadrotor dynamics," *Recent Advances in Aircraft Technology*, 2012, pp. 141–156.

[6] Park, S., Eun, W., and Shin, S. J., "Hybrid analysis for quadrotor type uav and modified blade element momentum theory considering gust and flight condition," *AIAA Scitech 2019 forum*, 2019, p. 1329.

[7] Shastry, A. K., Kothari, M., and Abhishek, A., "Generalized flight dynamic model of quadrotor using hybrid blade element momentum theory," *Journal of Aircraft*, Vol. 55, No. 5, 2018, pp. 2162–2168.

[8] Whidborne, J. F., Mendez, A. P., and Cooke, A., "Effect of Rotor Tilt on the Gust Rejection Properties of Multirotor Aircraft," *Drones*, Vol. 6, No. 10, 2022, p. 305.

[9] Bouabdallah, S., Noth, A., and Siegwart, R., "PID vs LQ control techniques applied to an indoor micro quadrotor," *2004 IEEE/RSJ International Conference on Intelligent Robots and Systems (IROS)(IEEE Cat. No. 04CH37566)*, Vol. 3, IEEE, 2004, pp. 2451–2456.

[10] Adigbli, P., Grand, C., Mouret, J.-B., and Doncieux, S., "Nonlinear attitude and position control of a micro quadrotor using sliding mode and backstepping techniques," *7th European Micro Air Vehicle Conference (MAV07)*, 2007, pp. 1–9.

[11] Park, O., Shin, H.-S., and Thourdos, A., "Evolutionary game theory based multi-objective optimization for control allocation of over-actuated system," *IFAC-PapersOnLine*, Vol. 52, No. 12, 2019, pp. 310–315.

[12] Lee, D., Jin Kim, H., and Sastry, S., "Feedback linearization vs. adaptive sliding mode control for a quadrotor helicopter," *International Journal of control, Automation and systems*, Vol. 7, 2009, pp. 419–428.

[13] Besnard, L., Shtessel, Y. B., and Landrum, B., "Quadrotor vehicle control via sliding mode controller driven by sliding mode disturbance observer," *Journal of the Franklin Institute*, Vol. 349, No. 2, 2012, pp. 658–684.

[14] Seddon, J. M., and Newman, S., *Basic helicopter aerodynamics*, John Wiley & Sons, 2011.

[15] Bramwell, A. R. S., Balmford, D., and Done, G., *Bramwell's helicopter dynamics*, Elsevier, 2001.

[16] Stevens, B. L., Lewis, F. L., and Johnson, E. N., *Aircraft control and simulation: dynamics, controls design, and autonomous systems*, John Wiley & Sons, 2015.

[17] Beard, R. W., and McLain, T. W., *Small unmanned aircraft: Theory and practice*, Princeton university press, 2012.

[18] Khalil, H. K., *Nonlinear control*, Vol. 406, Pearson New York, 2015.

[19] Lombaerts, T., Kaneshige, J., Schuet, S., Aponso, B. L., Shish, K. H., and Hardy, G., "Dynamic inversion based full envelope flight control for an eVTOL vehicle using a unified framework," *AIAA Scitech 2020 Forum*, 2020, p. 1619.

[20] Martinez Martinez, V., "Modelling of the flight dynamics of a quadrotor helicopter," , 2007.

[21] Standingford, D., Sequeira, C., Allan, M., Rider, C., Furse, G., and Sharpe, J., "Validating airspace CFD models for drone operation with flight test data," *33th Congress of the international countil of the aeronautical sciences, ICAS*, 2022.



https://dspace.org/

Dynamics modeling of multirotor type UAV with the blade element momentum theory and nonlinear controller design for a wind environment

Park, On; Shin, Hyo-Sang

2024-01-04
American Institute of Aeronautics and Astronautics (AIAA)
https://doi.org/10.2514/6.2024-2875
Park O, Shin HS. (2024) Dynamics modeling of multirotor type UAV with the blade element momentum theory and nonlinear controller design for a wind environment. In: AIAA SCITECH 2024 Forum, 8-12 January 2024, Orlando, USA. Paper number AIAA 2024-2875

Downloaded from a DSpace repository. https://dspace.org/